J Mater Sci (2006) 41:4537–4542
DOI 10.1007/s10853-006-0148-y

Fabrication and characterization of Au-nanoparticle/W-nanodendrite structures on Al_2O_3 substrate

Guoqiang Xie · Minghui Song · Kazuo Furuya

Received: 1 December 2005 / Accepted: 13 February 2006 / Published online: 6 July 2006

Abstract An Au-nanoparticle/W-nanodendrite compound structure was fabricated on an insulator Al_2O_3 substrate using an electron-beam-induced deposition (EBID) process combined with an ion sputtering method. The as-fabricated compound structures were characterized and analyzed using conventional and high-resolution transmission electron microscopy (CTEM and HRTEM) and X-ray energy dispersive spectroscopy (EDS). W-nanodendrite structures with the tips of 3 nm were grown self-standing at the edge of the Al_2O_3 substrate at positions separated from each other in distance of several nanometers. Au-nanoparticles with a grain size of 2.1 nm were uniformly distributed on the W-nanodendrites. The Au-nanoparticles were determined to be the equilibrium phase of Au with the face-centered cubic (fcc) structure.

Introduction

Metal nanostructures are of great importance in nanotechnology due to their potential applications as building blocks in optoelectronic devices, catalysis, chemical sensors, and other areas. Formation of nanostructures with controlled size and morphology has been the focus of intensive research in recent years. Such nanostructures are important in the development of nanoscale devices and in the exploitation of the properties of nanomaterials. The impact is greater for multi-element systems, as in the case of new nanostructured systems like Au/Ag [1], Au/Cu compound materials [2] and so on, which are used in catalysis, sensors, energy sources [3, 4] and in many other applications.

Platinum and platinum-group metals (such as palladium and rhodium) are excellent catalysts and have enjoyed widespread applications in the oil, chemical, and automotive industry for many years. However, Au has long been known as being catalytically far less active than other transition metals, as only a few reports of Au-based catalysis have been published during most of the 20th century [5]. A break-through came in the late 1980s when Haruta and co-workers made an exciting discovery: nanosized, supported Au exhibited unique catalytic properties. In the form of tiny clumps on a metal oxide or other support, Au can oxidize CO and catalyze a variety of other industrially important reactions at remarkably low temperatures [6, 7]. This discovery has attracted an intense research effort aimed at developing Au-based catalysts for industrial applications. Recently, it was found that, when dispersed as ultrafine particles and supported on metal or its oxides such as TiO_2, Au exhibits an extraordinary high activity for low-temperature catalytic combustion, partial oxidation of hydrocarbons, hydrogenation of unsaturated hydrocarbons, and reduction of nitrogen oxides [8–12]. The catalytic properties of Au depend on the support, the preparation method, and particularly the size of Au particles [13–18].

On the other hand, the studies have indicated that bimetallic bonding can induce significant changes in the

G. Xie (✉) · M. Song · K. Furuya
High Voltage Electron Microscopy Station, National Institute for Materials Science, 3-13 Sakura, Tsukuba 305-0003, Japan
e-mail: xiegq@imr.tohoku.ac.jp

G. Xie
Institute for Materials Research, Tohoku University, Katahira 2-1-1, Aoba-Ku, Sendai 980-8577, Japan

properties of the surface, producing in many cases catalysts that have superior activity and/or selectivity [1, 2, 18, 19].

In the present study, using an electron-beam-induced deposition (EBID) process combined with ion sputtering method, an Au-nanoparticle/W-nanodendrite compound structure was fabricated on an insulator Al_2O_3 substrate. The as-fabricated structures were characterized and analyzed using conventional and high-resolution transmission electron microscopy (CTEM and HRTEM) and X-ray energy dispersive spectroscopy (EDS).

Experimental methods

Crystalline Al_2O_3 thin film specimens suitable for TEM observation were used as substrates. The specimens were prepared from commercially obtained wafers by means of dimpling and argon ion milling.

With the Al_2O_3 thin film substrates, W-nanodendrites were grown using an EBID process. The EBID process was carried out in a high-voltage transmission electron microscope (HVTEM, JEM-ARM 1000, JEOL, Japan). Accelerating voltage used was 1000 kV. Base pressure in column was lower than 2×10^{-6} Pa. A cold trap filled with liquid nitrogen near the specimen holder was used to eliminate contamination by residual gases in the column of the TEM. A gas introduction system including a nozzle and a reservoir of precursor source was installed on this microscope. The nozzle was located within 2 mm of the specimen. The inner diameter of the nozzle was smaller than 0.1 mm. $W(CO)_6$ was used as a precursor. The flux of the gas near the specimen surface was estimated to be 2×10^{-7} Pa m^3 s^{-1} assuming molecular flow conditions. At this flux, the measured value of the background pressure of the chamber did not change detectably. The current density of electron beam for irradiating the specimens estimated by measuring total intensity and size of electron beam at a working condition, was 5.9 A cm^{-2}. The size of electron beam during irradiation was about 2000 nm.

After the W-nanodendrites were grown, sequentially, Au nanoparticles were deposited on the W-nanodendrites using an ion sputtering method in a quick auto coater system (Mode JFC 1500, JEOL, Japan), and formed a compound nanoparticle/nanodendrite structure. The pressure in chamber for ion sputtering was lower than 1×10^{-1} Pa. The anodic voltage used during sputtering was 1 kV, and anodic current was 7 mA. The ion sputtering time was 7 s.

The as-fabricated structures were observed and analyzed in situ or after the fabrication using a JEM-ARM1000 TEM operated at 1000 kV and an EDS attached to a JEM-2100F TEM. All the experiments were carried out at room temperature.

Results and discussion

Fabrication of W-nanodendrite structures

With the EBID process, W deposition on an insulator Al_2O_3 substrate was carried out in the TEM. The W-nanodendrite structures were observed to grow in the area of electron-beam irradiation. Figure 1 shows TEM micrographs of W-nanodendrite structures grown on an Al_2O_3 substrate. Figure 1a presents TEM image of Al_2O_3 substrate prior to W-nanodendrites formation, and Fig. 1b shows the substrate after W-nanodendrites have grown. The electron beam was defocused to a size of about 2000 nm, corresponding to a current density of

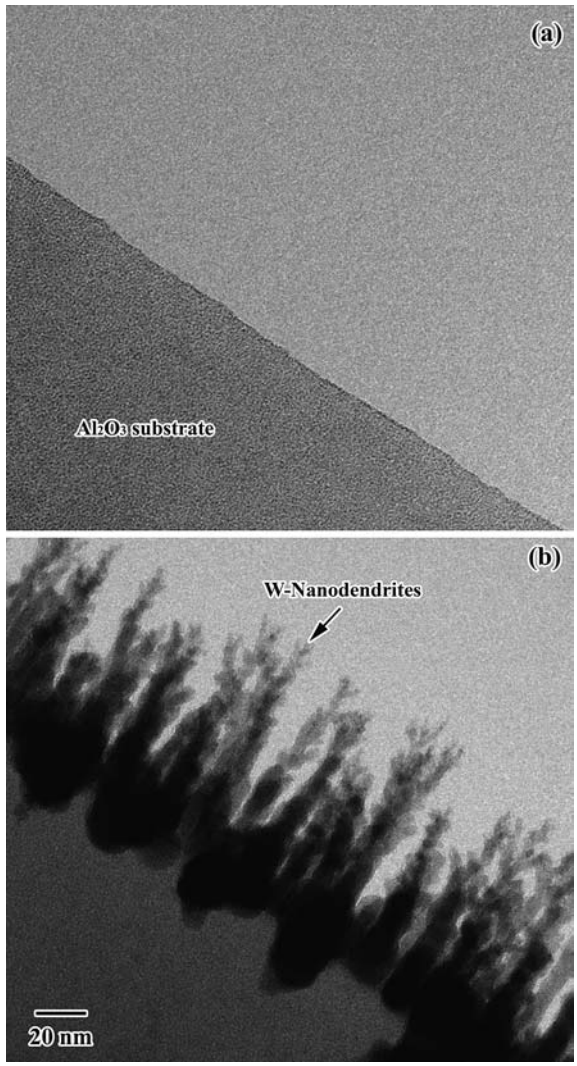

Fig. 1 TEM micrographs of W-nanodendrite structures grown on the surface of an Al_2O_3 substrate using an EBID process. (**a**) prior to W-nanodendrites formation; (**b**) after W-nanodendrites growth with an electron beam irradiation time of 2 min to a fluence of 4.4×10^{21} cm^{-2}

5.9 A cm^{-2}, which was nearly constant over the irradiated area [20]. The irradiation time was 2 min, and the electron irradiation fluence was 4.4×10^{21} cm^{-2}. The electron beam irradiated the specimen from a direction perpendicular to the plane of the micrograph. The W-nanodendrites showed a tendency to grow at the edge of the substrate, as indicated in Fig. 1b. They were grown self-standing at positions separated from each other in distance of several nanometers. The W-nanodendrites had branches at the tips, as observed in Fig. 1b. The diameter of the W-nanodendrites became thicker near the substrate, which implied that the deposition occurred at both the tip and trunk. The typical thickness of the tips was less than 3 nm, as shown in Fig. 1b. The length of the nanodendrite structures increased with electron beam irradiation fluence (namely, electron beam irradiation time). Furthermore, the morphology and the growth process of the W-nanodendrite structures formed on the Al_2O_3 substrate exhibited no obvious differences with those grown on SiO_2 substrates as described in previous reports [21–23].

The chemical composition of the as-fabricated nanodendrite structures was examined using EDS microanalysis. Figure 2 shows an EDS spectrum obtained from the tip of the as-deposited nanodendrites corresponding to Fig. 1b after detaching the precursor source. The size of electron beam for the EDS analysis was approximately 10 nm. As expected, the peaks of W dominated the spectrum, which is shown in Fig. 2. Similar results were also obtained from the analyses of other nanodendrites.

The growth and morphology of the W-nanodendrite structures are considered to be attributed to a mechanism involving charge-up produced on the surface of the substrate, movement of the charges to and accumulation at the surface of the substrate and tips of the deposits [21, 24].

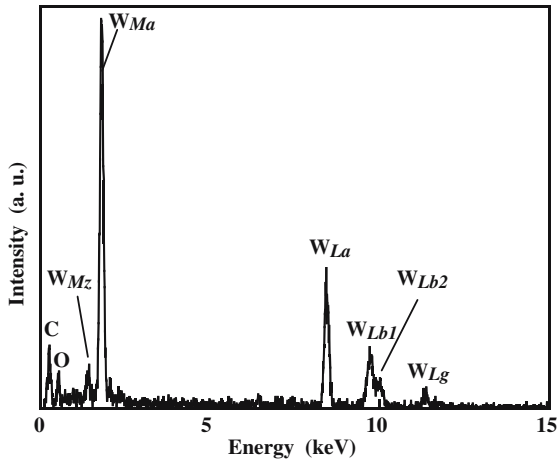

Fig. 2 EDS spectrum obtained from the tip of the as-fabricated W-nanodendrites corresponding to Fig. 1b. The size of electron beam for the EDS analysis is about 10 nm

It is well known that EBID is caused by the dissociation of molecules adsorbed to a surface by energetic electron beam. The molecule of a precursor is first adsorbed on surface of a substrate and then decomposed into volatile and non-volatile parts by further irradiation of the energetic beam. The non-volatile component accumulates to form a deposit, while the volatile component is pumped away by the vacuum system. The dissociation mechanism is complex and as yet not fully understood because of the huge number of excitation channels available even for small molecules. The details involving the decomposition have been proposed to be related to secondary electrons on the surface of a specimen produced by the incident electron beam and backscattered electrons in an EBID process [25, 26]. On the surface of an electrically grounded conductive substrate, the molecules adsorbed may or may not move, but will be distributed randomly and then be decomposed on the surface. Therefore, a compact deposit is usually formed [25–32]. On the other hand, in the case when the deposition is conducted on an insulator substrate, charge-up may take place on the surface. Hart et al. [33] had demonstrated that insulating specimens are charged in the beam owing to the emission of secondary electrons under energetic beam irradiation. The charge-up of the surface of a substrate has been considered to be a reason for the growth of carbon dendrite-like or filament-like structures on insulator substrates under electron beam irradiation [34, 35]. When specimens are exposed to electron bombardments, the molecules adsorbed to a surface of a substrate or near the surface in the irradiated area are polarized by irradiation from the incident electron beam [34]. The irradiated area on the insulator substrate is easily charged and forms a local electric field. Due to the Coulomb interaction in an electric field on the surface, these polarized molecules are attracted to the irradiated area. They are decomposed and form a deposit. The distribution of charges due to charge-up on the surface may not be even on a nanometer scale [24]. This unevenness may be due to the nanoscale roughness or atomic steps on the surface. Charges may accumulate on the surface of the substrate or the deposit, and tend to move to places with convex surface, such as a convex edge, especially sharp tips. The denser charges may be accumulated in these places so that the built-up electric field may be stronger than in the surrounding regions. Therefore, movable precursor molecules from both the surface and outside of the substrate may be attracted to these places. After a deposit is formed, charges may move and accumulate at its tip, hence the deposit will grow longer under the continued electron beam irradiation. Since the built-up electric field near a tip may not significantly influence the mobility of a molecule, the deposit grows at both its tip and its trunk part due to molecules coming to tips and trunk at the same time. The deposit will

grow thicker at its trunk part with increasing time and thus develop a dendrite morphology. Therefore, the movement and accumulation of charges play a key role in the formation of the dendrite structure.

Fabrication and characterization of Au-nanoparticle/W-nanodendrite structures

Au-nanoparticles were deposited on the W-nanodendrite structures on an insulator Al_2O_3 substrate, and a compound structure of the Au-nanoparticle/W-nanodendrite was fabricated by an ion sputtering method. Figure 3 shows a TEM micrograph of the as-fabricated Au-nanoparticle/W-nanodendrite compound structure on an Al_2O_3 substrate for an ion sputtering time of 7 s. It is observed that the nanoparticles were nearly uniformly distributed on the W-nanodendrite structures. The number density of the deposited Au-nanoparticles based on measuring 10 regions of 50×50 nm is 2.7×10^{12} cm^{-2}.

The as-fabricated Au-nanoparticle/W-nanodendrite compound structures were characterized using EDS analyses. Figure 4 shows an EDS spectrum obtained at the tip of the as-fabricated Au-nanoparticle/W-nanodendrite compound structures corresponding to Fig. 3. The size of electron beam for the EDS analysis was approximately 10 nm. Figure 4 shows that the peaks for Au and W dominate the spectrum although there are small amounts of C and O. Thus, it is confirmed that the desired element Au has been effectively incorporated in the nanometer-sized compound structures.

Further characterization of the as-fabricated Au-nanoparticle/W-nanodendrite compound structures was performed using HRTEM. Figure 5 shows an HRTEM

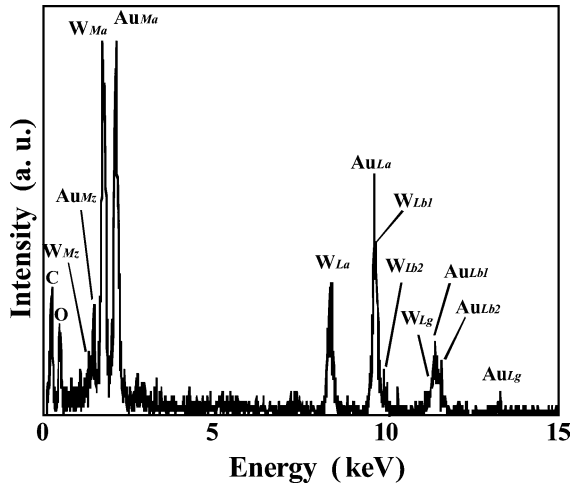

Fig. 4 EDS spectrum obtained from the tip of the as-fabricated Au-nanoparticle/W-nanodendrite compound structures corresponding to Fig. 3. The size of electron beam for the EDS analysis is about 10 nm

micrograph of some branches of the nanoparticle/nanodendrite compound structure fabricated with an electron beam irradiation fluence of 4.4×10^{21} cm^{-2} and an ion sputtering time of 7 s. The defocus value of the HRTEM image was taken as −49.4 nm, which corresponds to the Scherzer focus of −57 nm. Lattice fringes can be observed in the image. The lattice spacing in some regions measuring from this figure and other images was 0.22 nm. This is close to the lattice spacing 0.224 nm of {110} of bulk metal body-centered cubic (bcc) W crystals with a deviation smaller than 5%, as shown in Fig. 5. Moreover, lattice fringes with spacing $d = 0.22$ nm have inter-fringe angle of 60 degrees, as well as that of 90 degrees. They correspond

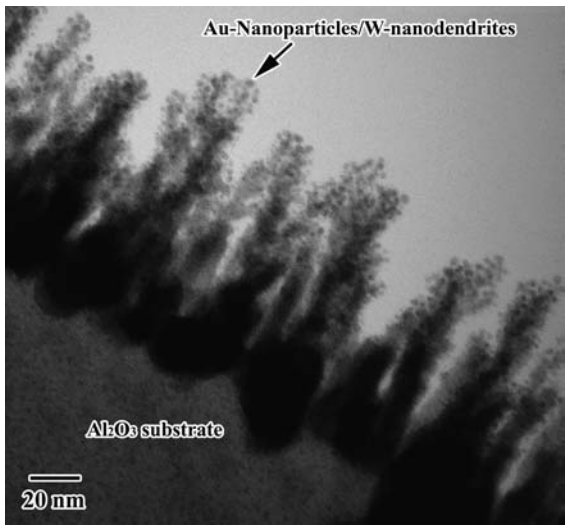

Fig. 3 TEM micrograph of the as-fabricated Au-nanoparticle/W-nanodendrite compound structures on an Al_2O_3 substrate for an ion sputtering time of 7 s

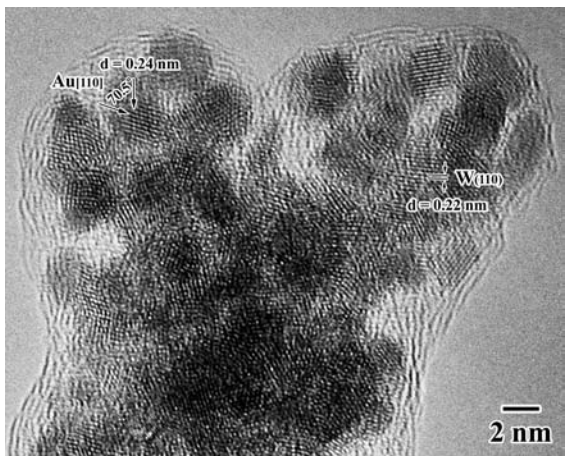

Fig. 5 An HRTEM micrograph of branches of the Au-nanoparticle/W-nanodendrite compound structures fabricated with an electron beam irradiation fluence of 4.4×10^{21} cm^{-2} and an ion sputtering time of 7 s

to the [111] and [001] zone axes of the bcc W structure, respectively. The details have been reported in previous papers [21, 23]. Furthermore, in some other regions in Fig. 5, the lattice spacing measured was 0.24 nm, which was close to the lattice spacing, 0.236 nm, for {111} bulk metal face-centered cubic (fcc) Au crystals. The lattice fringes with spacing $d = 0.24$ nm in some particles had an inter-fringe angle of 70.5 degrees, as indicated in Fig. 5. This is in agreement with the [110] zone axis for the fcc Au structure. The HRTEM micrographs taken from other regions or other Au-nanoparticle/W-nanodendrite compound structures also yielded similar results. From the HRTEM micrographs, the size of the Au-nanoparticles was measured for 207 particle diameters. The results of the measured nanoparticle size distribution is shown in Fig. 6. It is observed that there was a relatively narrow nanoparticle size distribution. The average nanoparticle size for the present ion sputtering conditions was 2.1 nm. The particle size can be easily controlled by controlling the ion sputtering time.

Conclusions

Using an EBID process combined with ion sputtering method, Au-nanoparticle/W-nanodendrite compound structures were successfully fabricated on an insulator Al_2O_3 substrate. The as-fabricated compound structures were characterized and analyzed using CTEM, HRTEM, and EDS. The W-nanodendrite structures with the tips in about 3 nm were grown self-standing at the edge of the Al_2O_3 substrate at positions separated from each other in distance of several nanometers. Au-nanoparticles with a grain size of 2.1 nm were uniformly distributed on the W-nanodendrites. The Au-nanoparticles were determined to be equilibrium phase of Au with fcc structure. These compound structures have potential use in the design of nanostructured materials for catalytic applications.

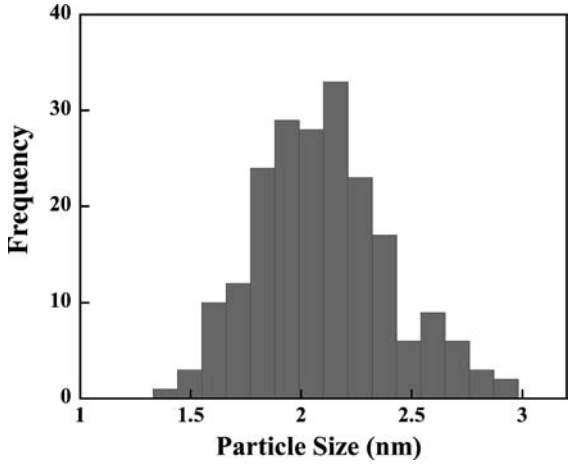

Fig. 6 The size distribution of Au particles in the Au-nanoparticle/W-nanodendrite compound structures fabricated with an electron beam irradiation fluence of 4.4×10^{21} cm^{-2} and an ion sputtering time of 7 s

References

1. Link S, Burda C, Wang ZL, El-Sayed MA (1999) J Chem Phys 11:1255
2. Pal U, Sanchez Ramirez JF, Liu HB, Medina A, Ascencio JA (2004) Appl Phys A 79:79
3. Ruiz A, Arbiol J, Cirera A, Cornet A, Morante JR (2002) Mater Sci Eng C 19:105
4. De Meijer RJ, Stapel C, Jones DG, Roberts PD, Rozendaal A, Macdonald WG, Chen KZ, Zhang ZK, Cui ZL, Zuo DH, Yang DZ (1997) Nanostruct Mater 8:205
5. Bond GC (2002) Catal Today 72:5
6. Haruta M, Yamada N, Kobayashi T, Iijima S (1989) J Catal 115:301
7. Haruta M (1997) Catal Today 36:153
8. Diebold U (2005) Surf Sci 578:1
9. Wang D, Hao Z, Cheng D, Shi X, Hu C (2003) J Mol Catal 200:229
10. Franceschetti A, Pennycook SJ, Pantelides ST (2003) Chem Phys Lett 374:471
11. Bulushev DA, Kiwi-Minsker L, Yuranov I, Suvorova EI, Buffat PA, Renken A (2002) J Catal 210:149
12. Akita T, Okumura M, Tanaka K, Kohyama M, Haruta M (2005) J Mater Sci 40:3101
13. Boccuzzi F, Chiorino A, Manzoli M, Lu P, Akita T, Ichikawa S, Haruta M (2001) J Catal 202:256
14. Meier DC, Goodman DW (2004) J Am Chem Soc 126:1892
15. Chen YJ, Yeh CT (2001) J Catal 200:59
16. Kozlov AI, Kozlova AP, Asakura K, Matsui Y, Kogure T, Shido T, Iwasawa Y (2000) J Catal 196:56
17. Arrii S, Morfin F, Renouprez AJ, Rousset JL (2004) J Am Chem Soc 126:1199
18. Wang A, Liu J, Lin S, Lin T, Mou C (2005) J Catal 233:1486
19. Liu P, Rodriguez JA, Muckerman JT, Hrbek J (2003) Surf Sci 530:L313
20. Song M, Mitsuishi K, Takeguchi M, Furuya K (2005) Appl Surf Sci 241:107
21. Xie GQ, Song M, Mitsuishi K, Furuya K (2005) J Nanosci Nanotechno 5:615
22. Xie GQ, Song M, Mitsuishi K, Furuya K (2005) Jpn J Appl Phys 44:5654
23. Xie GQ, Song M, Mitsuishi K, Furuya K (2005) Physica E 29:564
24. Song M, Mitsuishi K, Tanaka M, Takeguchi M, Shimojo M, Furuya K (2005) Appl Phys A 80:1431
25. Koops HWP, Weiel R, Kern DP, Baum TH (1988) J Vac Sci Technol B 6B:477
26. Hoyle PC, Cleaver JRA, Ahmed H (1996) J Vac Sci Technol B 14:662

27. Mitsuishi K, Shimojo M, Han M, Furuya K (2003) Appl Phys Lett 83:2064
28. Dong LX, Arai F, Fukuda T (2002) Appl Phys Lett 81:1919
29. Matsui S, Kaito T, Fujita J, Komura M, Kanda K, Haruyama Y (2000) J Vac Sci Technol B 18:3181
30. Utke I, Hoffmann P, Dwir B, Leifer K, Kapon E, Doppelt P (2000) J Vac Sci Technol B 18:3168
31. Hiroshima H, Suzuki N, Ogawa N, Komuro M (1999) Jpn J Appl Phys 38:7135
32. Kohlmann-Von Platen KT, Chlebek J, Weiss M, Reimer K, Oertel H, Brunger WH (1993) J Vac Sci Technol B 11:2219
33. Hart RK, Kassner TF, Maurin JK (1970) Phil Mag 21:453
34. Banhart F (1995) Phys Rev E 52:5156
35. Wang HZ, Liu XH, Yang XJ, Wang X (2001) Mater Sci Eng A 311:180